Retrieval of Land Surface Albedo from Satellite Observations: A Simulation Study

SHUNLIN LIANG

Department of Geography, University of Maryland at College Park, College Park, Maryland

ALAN H. STRAHLER

Department of Geography and Center for Remote Sensing, Boston University, Boston, Massachusetts

CHARLES WALTHALL

USDA Agricultural Research Service, Beltsville, Maryland

(Manuscript received 27 February 1998, in final form 26 August 1998)

ABSTRACT

Land surface albedo is a critical parameter affecting the earth's climate and is required by global and regional climatic modeling and surface energy balance monitoring. Surface albedo retrieved from satellite observations at one atmospheric condition may not be suitable for application to other atmospheric conditions. In this paper the authors separate the apparent surface albedo from the inherent surface albedo, which is independent of atmospheric conditions, based on extensive radiative transfer simulations under a variety of atmospheric conditions. The results show that spectral inherent albedos are different from spectral apparent albedos in many cases. Total shortwave apparent albedos under both clear and cloudy conditions are also significantly different from their inherent total shortwave albedos.

The conversion coefficients of the surface inherent narrowband albedos derived from the MODIS (Moderate-Resolution Imaging Spectroradiometer) and the MISR (Multiangle Imaging Spectroradiometer) instruments to the surface broadband inherent albedo are reported. A new approach of predicting broadband surface inherent albedos from MODIS or MISR top of atmosphere (TOA) narrowband albedos using a neural network is proposed. The simulations show that surface total shortwave and near-infrared inherent albedos can be predicted accurately from TOA narrowband albedos without atmospheric information, whereas visible inherent albedo cannot.

1. Introduction

Land surface albedo is a critical parameter affecting the earth's climate (Cess 1978; Dickinson 1983). For many general circulation models (GCMs), both visible (0.4–0.7 μm) and near-infrared (0.7–5.0 μm) albedos are needed, whereas the surface energy balance studies typically require broadband shortwave (0.25–5.0 μm) albedo. Although surface albedo has been routinely observed for a long time and different approaches have been explored (Walthall et al. 1985; Pinty and Ramond 1987; Kimes and Holben 1992; Ranson et al. 1991; Li and Garand 1994), a global map of surface albedo with high accuracy is not simply available right now. It has been well recognized that surface albedo is among the main radiative uncertainties in current climate modeling. Most GCMs are still using prescribed fields of surface albedo that are often 5%–15% in error from place to place and time to time (Dorman and Sellers 1989; Sato et al. 1989).

Both MODIS (Moderate-Resolution Imaging Spectroradiometer) and MISR (Multiangle Imaging Spectroradiometer) science teams in the EOS (Earth Observing System) program will provide the surface albedo products in individual spectral bands. The MISR team will also generate visible albedo (Diner 1996), and the MODIS team is to produce all three broadband albedo products: visible, near-infrared, and total shortwave (Strahler et al. 1996). The MODIS and MISR algorithms are quite different in retrieval of surface reflectance from top of atmosphere (TOA) measurements through atmospheric correction. MODIS has the advantage of many spectral bands. This leads directly to the retrieval of many critical parameters required by atmospheric correction, such as water vapor profiles, column ozone, and aerosol optical depth. MISR relies on the principle of multiple view angles to observe the along-track angular scattering of aerosol. (Ozone and water vapor will be obtained from external sources.) MODIS also has a

Corresponding author address: Shunlin Liang, Laboratory for Global Remote Sensing Studies, Department of Geography, University of Maryland, College Park, MD 20742.
E-mail: sliang@geog.umd.edu

much greater cross-track scan width that leads to global coverage every two days, while MISR requires nine days.

The contrasting principles of these instruments determine the fundamental characterization of their albedo retrieval algorithms as well. MISR will retrieve albedo from a single suite of nine multiangle measurements made within a 6-min period, while the MODIS algorithm relies on assembling multiangle data from both MODIS and MISR for a 16-day period. Both algorithms calculate albedo by retrieving the surface bidirectional reflectance distribution function (BRDF) using relatively simple semiempirical or empirical mathematical functions known to fit the shapes of observed BRDFs well.

Surface broadband albedos are not sole measures of surface reflective properties, since they also depend on the atmospheric conditions. The downward irradiance distribution at the bottom of the atmosphere is the weighting function for converting spectral albedos to broadband albedos, and different atmospheric conditions have different downward irradiance distributions. Thus, surface broadband albedos retrieved under one specific atmospheric condition may not be applicable to other atmospheric conditions.

In this study, we contrast two albedo measures. Apparent albedo is simply the albedo that is observed given a particular atmospheric state. Inherent albedo is the directional-hemispherical surface reflectance integrated from surface BRDF over all viewing angles. It is completely independent of the atmospheric conditions. The apparent albedos under specific atmospheric conditions can be linked to the inherent albedo.

Converting narrowband surface albedos from satellite observations to broadband surface albedos is straightforward, but it involves an atmospheric correction procedure that converts TOA narrowband radiances into narrowband surface albedos. In this study, we find that it is also possible to derive surface albedos directly from TOA observations without performing any atmospheric correction. This idea stems from earlier studies (Chen and Ohring 1984; Pinker 1985; Koepke and Kriebel 1987; Li and Garand 1994) that linearly relate TOA albedo to surface albedos. As we just discussed, surface broadband albedo depends on the surface spectral reflectance as well as the atmospheric conditions. TOA albedo contains both information on surface reflectance and the atmospheric optical properties, which implies that it is possible for us to predict the broadband albedo using TOA narrowband albedos directly without performing any atmospheric corrections.

In this study, we utilize extensive radiative transfer simulations using MODTRAN 3.5 (Berk et al. 1989; Anderson 1996) and spherical harmonics discrete ordinate method (SHDOM) (Evans 1998) computer codes. A series of representative atmospheric and surface conditions were input into MODTRAN and the TOA narrowband albedos of MODIS and MISR were related to three broadband surface inherent albedos using polynomial regression and a feed-forward neural network technique. The relations between broadband surface inherent albedos and apparent albedos under different atmospheric conditions were also examined.

We will start by discussing different albedo concepts to illustrate why the surface albedo depends on the atmospheric conditions. We then introduce the shortwave database simulated by using MODTRAN, and the feed-forward neural network. Data analyses will be then given in the last section.

2. Definitions of albedos

Different terminologies have been used in the literature. It is necessary to define albedo in a systematic way in this study. It is also important to demonstrate why surface albedo changes under different atmospheric conditions and how we can solve this problem. In the following, inherent albedo is a sole measure of the surface reflectivity, and apparent albedo depends also on the atmospheric conditions.

Let us first define the surface spectral inherent albedo $\rho_I(\theta_i; \lambda)$ at any solar zenith angle θ_i and wavelength λ,

$$\rho_I(\theta_i; \lambda) = \frac{1}{\pi}\int_0^1 \int_0^{2\pi} R(-\theta_i, \theta, \phi)\mu \, d\mu \, d\phi, \quad (1)$$

where $\mu = \cos(\theta)$ and $R(-\theta_i, \theta, \phi)$ is the bidirectional reflectance factor (BRF). Sometimes, bidirectional reflectance distribution function is referred to as BRF (Strahler et al. 1996), although it is equal to BRF divided by π (Diner et al. 1996; Strahler et al. 1996). Both BRF and BRDF are the sole measure of the surface reflectivity at the viewing direction given specific direct illuminations. Albedo defined in (1) is referred to as ''black-sky'' albedo in the MODIS ATBD (Algorithm Theoretical Basis Document) (Strahler et al. 1996) and ''directional-hemispherical reflectance'' in the MISR ATBD (Diner 1996).

Spectral apparent albedo (ρ_A) is defined as the ratio of upwelling irradiance $F_u(\theta_i; \lambda)$ to downward irradiance $F_d(\theta_i; \lambda)$ at the solar zenith angle θ_i:

$$\rho_A(\theta_i, \lambda) = \frac{F_u(\theta_i; \lambda)}{F_d(\theta_i; \lambda)} = \frac{\frac{1}{\pi}\int_0^1 \int_0^{2\pi} \int_0^1 \int_0^{2\pi} R(-\mu', \mu, \phi', \phi) L^{\mathrm{inc}}(-\mu', -\mu_i, \phi', \phi_i)\mu\mu' \, d\mu' \, d\phi' \, d\mu \, d\phi}{\int_0^1 \int_0^{2\pi} L^{\mathrm{inc}}(-\mu', -\mu_i, \phi', \phi_i)\mu' \, d\mu' \, d\phi'}, \quad (2)$$

where $L^{\mathrm{inc}}(-\mu', -\mu_i, \phi', \phi_i)$ is the total downward radiance (direct plus diffuse) illuminated to the surface; it is obviously a function of the atmospheric conditions. It is called bihemispherical reflectance in the MISR ATBD (Diner 1996).

Apparent albedo in any waveband is defined similarly:

$$\rho_A(\theta_i; \Lambda) = \frac{F_u(\theta_i; \Lambda)}{F_d(\theta_i; \Lambda)} = \frac{\int_{\lambda_1}^{\lambda_2} F_u(\theta_i; \lambda)\, d\lambda}{\int_{\lambda_1}^{\lambda_2} F_d(\theta_i; \lambda)\, d\lambda}, \qquad (3)$$

where Λ is denoted to be the waveband from wavelegth λ_1 to wavelength λ_2 [Λ:(λ_1, λ_2)]. If Λ:(0.25 μm–5.0 μm), $\rho(\theta_i; \Lambda)$ is the total shortwave broadband albedo. The waverange Λ:(0.4 μm–0.7μm) and Λ:(0.7 μm–5.0 μm) correspond to visible and near-infrared albedos, respectively. Note that albedo is a dimensionless quantity. From the above definition, we can see that apparent albedo in any waveband is an average of that at every wavelength $\rho(\theta_i; \lambda)$ weighted by the proportional spectral downward irradiance:

$$\rho_A(\theta_i; \Lambda) = \frac{\int_{\lambda_1}^{\lambda_2} F_d(\theta_i; \lambda)\rho_A(\theta_i; \lambda)\, d\lambda}{\int_{\lambda_1}^{\lambda_2} F_d(\theta_i; \lambda)\, d\lambda}$$
$$= \int_{\lambda_1}^{\lambda_2} \frac{F_d(\theta_i; \lambda)}{F_d(\theta_i; \Lambda)}\rho_A(\theta_i; \lambda)\, d\lambda. \qquad (4)$$

Both MODIS and MISR are narrowband sensors. To calculate albedo in the wave range Λ from narrowband observations, we can either predict total upwelling irradiance $F_u(\theta_i; \Lambda)$ and downward irradiance $F_d(\theta_i; \Lambda)$ from narrowband irradiance or predict albedo directly from narrowband albedos:

$$\rho_A(\theta_i; \Lambda) = \frac{f_1[F_u(\theta_i; \Lambda_1), \cdots F_u(\theta_i, \Lambda_j)]}{f_2[F_d(\theta_i, \Lambda_1), \cdots F_d(\theta_i, \Lambda_j)]} \qquad (5)$$

or

$$\rho_A(\theta_i; \Lambda) = f_3[\rho_A(\theta_i; \Lambda_1), \cdots \rho_A(\theta_i; \Lambda_j)], \qquad (6)$$

where $\Lambda_1, \ldots, \Lambda_j$ represent j bands, with $j = 4$ for MISR and $j = 7$ for MODIS in the shortwave range. The transformation functions $f_i(\,)$ generally depend on the atmospheric conditions. Measurements indicate that land surface albedos under clear-sky conditions are more variable than those under cloudy conditions (Pinker 1985; Bastable et al. 1993).

Because apparent albedo values are derived under a specific atmospheric condition, we define the surface broadband inherent albedo as the ratio of upwelling irradiance from the surface that is illuminated by an unattenuated direct beam to the surface downward unattenuated irradiance, which is equal to the TOA solar extraterrestrial irradiance $F_0(\theta_i, \lambda)$,

$$\rho_I(\theta_i; \Lambda) = \frac{\int_{\lambda_1}^{\lambda_2} F_0(\theta_i, \lambda)\rho_I(\theta_i; \lambda)\, d\lambda}{\int_{\lambda_1}^{\lambda_2} F_0(\theta_i, \lambda)\, d\lambda}, \qquad (7)$$

where $\rho_I(\theta_i; \lambda)$ is defined in (1). From above definitions, we can see that surface broadband inherent albedo is completely independent of atmospheric conditions and therefore a measure of surface inherent reflectance properties. It is evident that the surface inherent albedo actually would be equivalent to apparent albedo under vacuum condition. If the figures/tables/formulas are provided to link apparent albedos with inherent albedos, the user can directly use the inherent albedo products from satellite observations.

3. MODTRAN simulation database

MODTRAN has been widely used in different applications of satellite remote sensing. For example, both MODIS and MISR (Advanced Spaceborne Thermal Emission and Reflection Radiometer) instrument science teams are using MODTRAN for the land surface temperature retrievals (Wan 1996; Palluconi et al. 1996). We have modified the output from the latest version of MODTRAN3.5 for our irradiance calculations with the help of MODTRAN developers.

A total of 20 surface reflectance spectra were input into MODTRAN from the USGS digital spectral library (Clark et al. 1993) and from measurements by Dr. J. Salisbury at The Johns Hopkins University. They have different wavelength dependence and magnitude, from vegetation canopies (low albedos) to snow and frost (high albedos) (Fig. 1). Since angular dependences of these surface reflectance spectra are not available, we simply assume these surface cover types are Lambertian (isotropic in reflectance). The Lambertian assumption may be far away from actual situations. To make simulations more realistic, however, we scaled these surface spectra to represent the dependences on the solar zenith angle according to a formula derived by Dickinson (1983), which has been adapted by the Clouds and the Earth's Radiant Energy System (CERES) instrument science team (Wielicki and Barkstrom 1996). To be precise, MODTRAN was run with isotropic reflectance in different viewing directions, but with reflectance varying as a function of solar zenith angle.

Four visibility values were used for different aerosol loadings: 5, 15, 35, and 70 km. A visibility of 5 km represents a very hazy atmospheric condition and 70-km visibility represents a very clear atmospheric condition. Five default aerosol models available in MODTRAN 3.5 were used: rural, maritime, urban, tropospheric, and desert. Twelve different water vapor profiles from the Tropical Ocean Global Atmosphere Coupled Ocean–Atmosphere Response Experiment (TOGA COARE) project (Loehrer et al. 1996) were

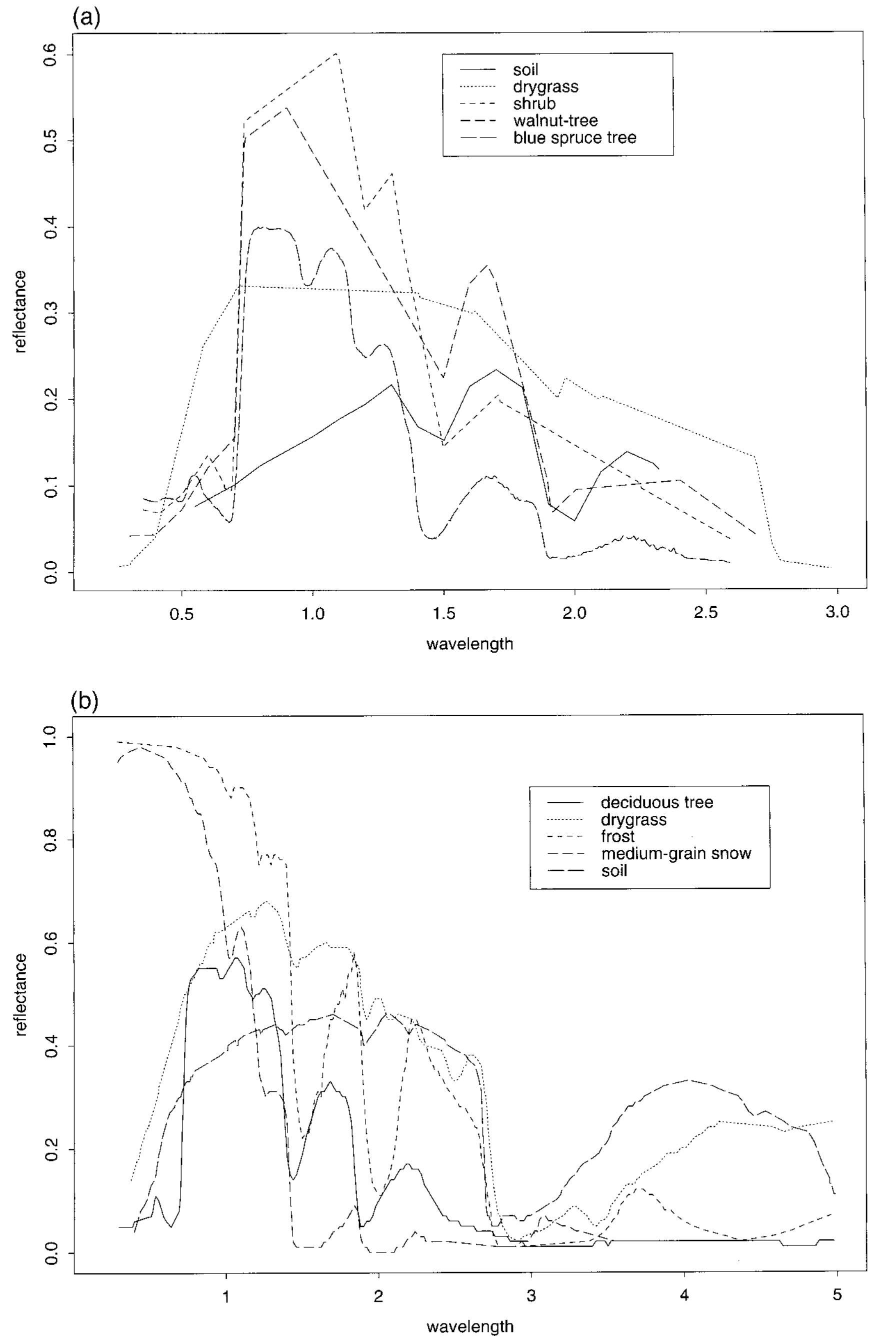

FIG. 1. Surface reflectance spectra used in the MODTRAN simulations.

used with the total precipitable water content from 0.41 to 6.05 cm. These profiles are over tropical oceans, which may be different from actual profiles over land. The purpose here is to simulate the humid atmospheric conditions. They are certainly better than any artificial humid conditions used in some simulations. A range of eight solar zenith angles was also considered (11.4°, 26.1°, 40.3°, 53.7°, 65.9°, 76.3°, 84.2°, 88.9°). These angles are Gauss–Laguerre abscissas.

To examine the difference between surface apparent albedos under cloudy conditions and surface inherent albedoes, five types of default clouds provided in the MODTRAN code were used: cumulus, altostratus, stratus, stratus/stratocumulus, and nimbostratus, each with different cloud optical depths and scattering properties.

Multiple scattering was calculated using the discrete ordinate (DISORT) mode in MODTRAN, which is a widely used code for atmospheric and surface radiative

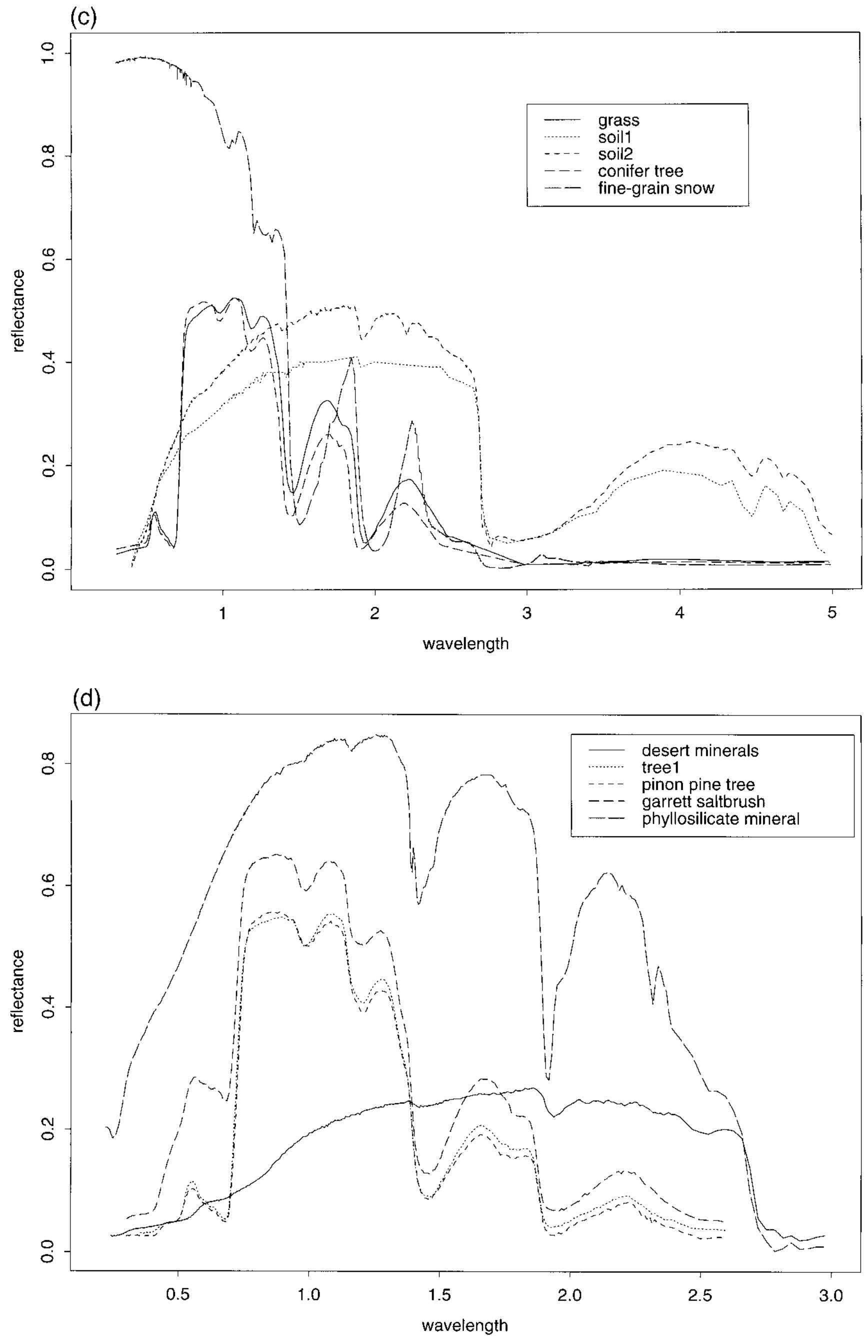

FIG. 1. (*Continued*)

transfer calculations (Stamnes et al. 1988; Tsay et al. 1989; Tsay and Stamnes 1992; Lindner 1988; Lummerzheim et al. 1989; Liang and Strahler 1994; Liang and Lewis 1996; Liang and Townshend 1996a,b). All calculations were carried out in the wavenumber range 2000–50 000 (corresponding to the wavelength range 0.20–5.00 μm) at 1 cm^{-1} (wavenumber) intervals. The outputs included TOA irradiance, TOA nadir reflectance, and surface irradiance. The outputs were then integrated with nominal sensor spectral response functions to obtain narrowband albedos for the MODIS and ASTER sensors.

4. Neural network and albedo retrieval

Artificial neural-network prediction has been used in a number of remote sensing applications (Atkinson and Tatnall 1997; Foody et al. 1997; Abuelgasim et al.

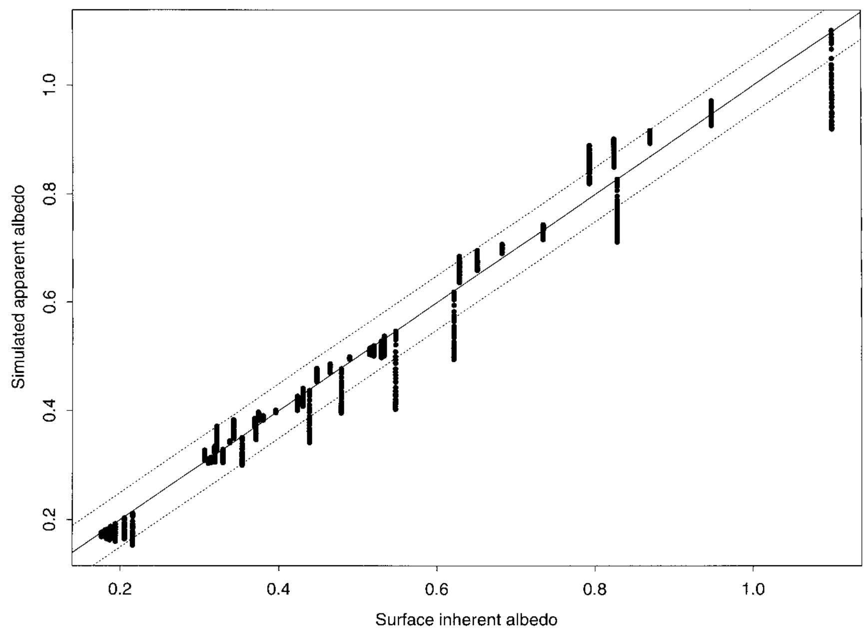

FIG. 2. Comparison of surface spectral inherent albedos with apparent albedos under different clear-sky conditions.

1996). The original motivation for neural networks was to mimic the possible learning behavior of the human brain. However, neural network studies have become increasingly artificial and are now not thought to be plausible as biological models. A feed-forward neural network contains many units connected to each other in such a way that they can be labeled from inputs to outputs. A feed-forward neural network is a "black-box" method. It provides a prediction for any input but no readily interpretable explanation for that prediction. As such, it loses some of the power of linear statistical models in statistical inference. However, it provides us a flexible way to generalize linear regression functions. It can be seen as a way to parameterize a fairly general nonlinear function.

The function we used in this study is called *nnet*( ) associated with the statistical package S-plus. The detailed descriptions of the function and augment specifications can be found elsewhere (Venables and Ripley 1994).

As illustrated in section 2, broadband surface albedo depends on surface spectral reflectance as well as atmospheric conditions. A TOA albedo contains information on both surface reflectance and atmospheric optical properties, which implies that it is possible to predict broadband surface albedo using TOA narrowband albedos without performing direct atmospheric correction. In our study, we use a feed-forward neural network to link TOA narrowband albedos as well as atmospheric parameters to three broadband albedos. Several neural network predictors can be created. First, suppose we have ancillary information about surface and atmospheric conditions. In this case, the model for surface broadband (visible, near-IR, or total shortwave) inherent albedo $R(\theta_i)$ at the solar zenith angle θ_i will look like

$$R(\theta_i) = f(\alpha_1, \ldots, \alpha_N, \Psi_a, \theta_i), \tag{8}$$

where N is the number of narrow bands, $\alpha_1, \ldots, \alpha_N$ are TOA albedos, which are defined as

$$\alpha_n = \frac{\pi^* L_n}{F_0^n \cos(\theta_i)}, \tag{9}$$

where L_n and F_0^n are upwelling radiance received by the sensor at the top of the atmosphere and solar TOA extraterrestrial downward irradiance at band n and $n = 1, \ldots, N$. The symbol Ψ_a denotes a set of atmospheric parameters, such as aerosol optical depth, water vapor content, CO_2, and O_3 contents.

In reality, we may not have all parameters about the atmospheric conditions. For example, the MODIS team will produce a global water vapor content product, but aerosol optical depths will be provided only over densely vegetated areas. The MISR team does not generate a water vapor content product, and the aerosol optical

TABLE 1. Parameters of the surface BRF.

Case	R_0	k	g
1	0.076	0.648	−0.290
2	0.238	0.668	0.015
3	0.357	0.879	−0.045
4	0.538	0.826	0.027
5	0.699	0.805	0.00097

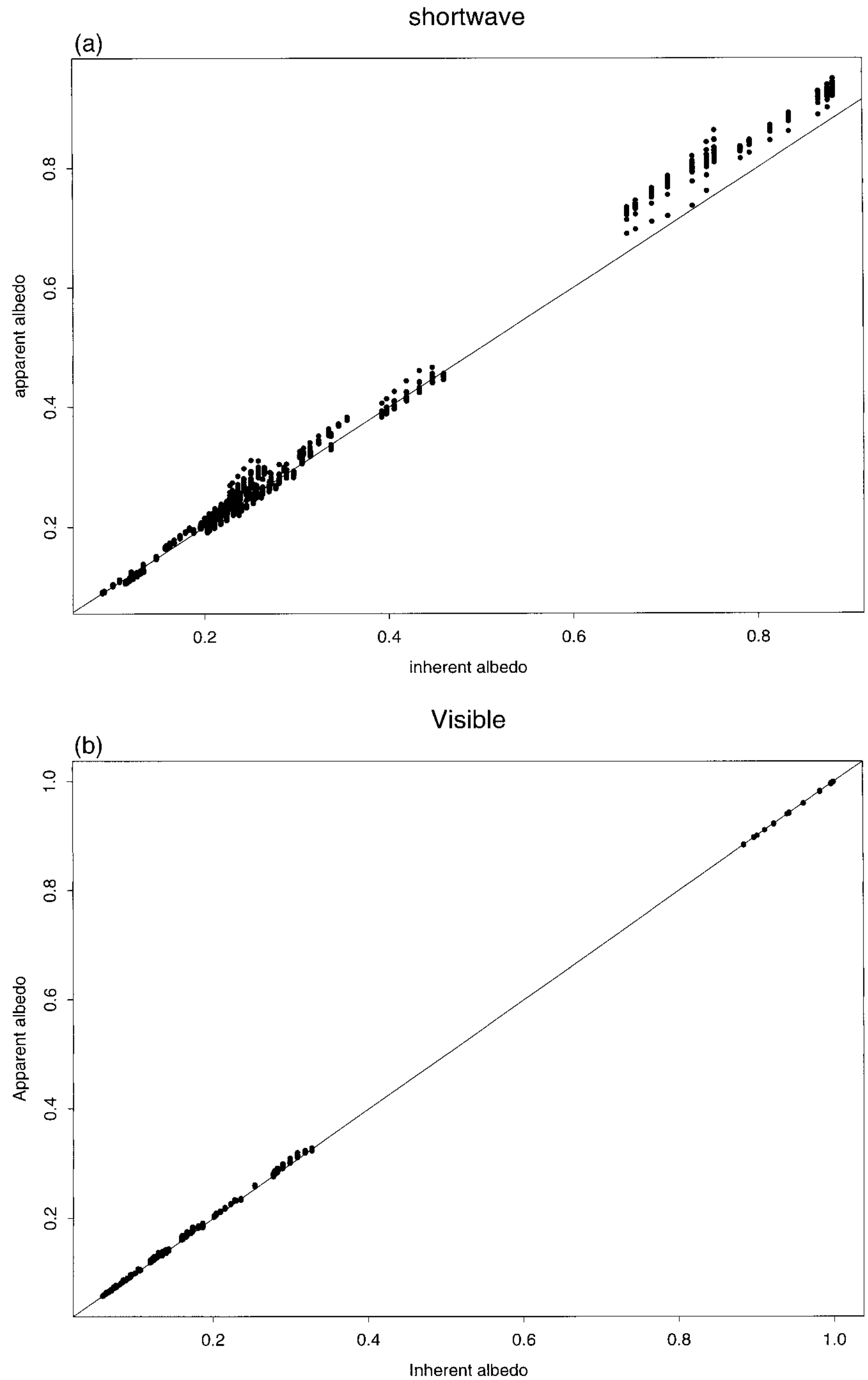

FIG. 3. Surface broadband inherent albedos and apparent albedos under different clear-sky conditions: (a) shortwave; (b) visible.

depth and aerosol model are available only over flat terrain. The alternative model is

$$R(\theta_i) = f(\alpha_1, \ldots, \alpha_N, \theta_i). \tag{10}$$

Since each product is associated with uncertainties, detailed sensitivity studies need to be conducted to determine the best model for the global applications.

5. Data analysis

a. Inherent and apparent albedos

We have defined both spectral and waveband apparent albedos (2), (3), which illustrate two scaling processes from inherent albedo. One is angular scaling, another is spectral scaling. Different angular distributions of sky

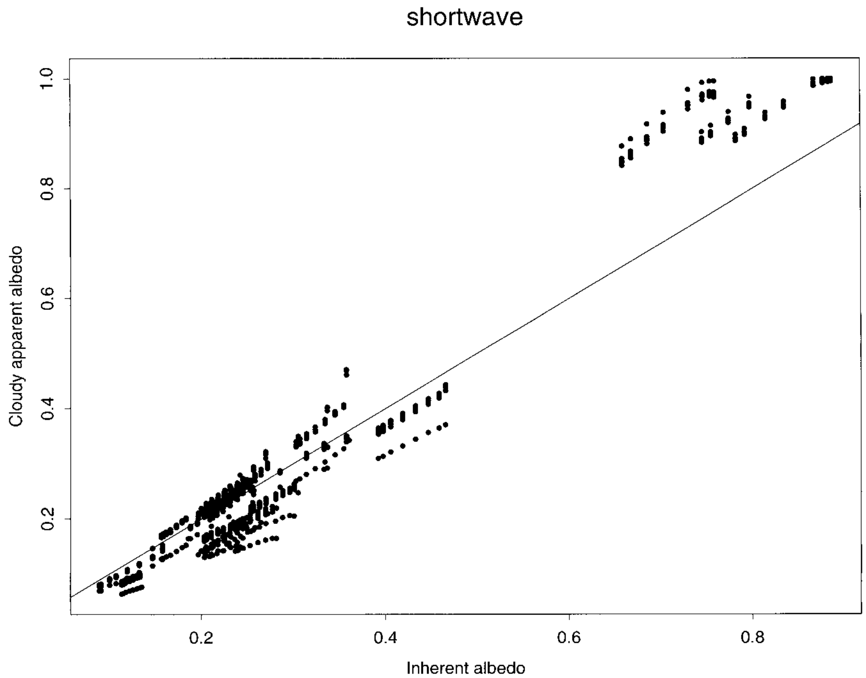

FIG. 4. Prediction of surface shortwave inherent albedos from MODIS narrowband TOA albedos using polynomial regression and a neural network.

radiance in conjunction with surface BRDF produce different apparent albedos. Different spectral distributions of the downward irradiance generate different broadband apparent albedos.

To show the differences between the surface spectral inherent albedo and apparent albedo under different conditions, we ran the radiative transfer code SHDOM (Evans 1998) for an aerosol atmosphere over a non-

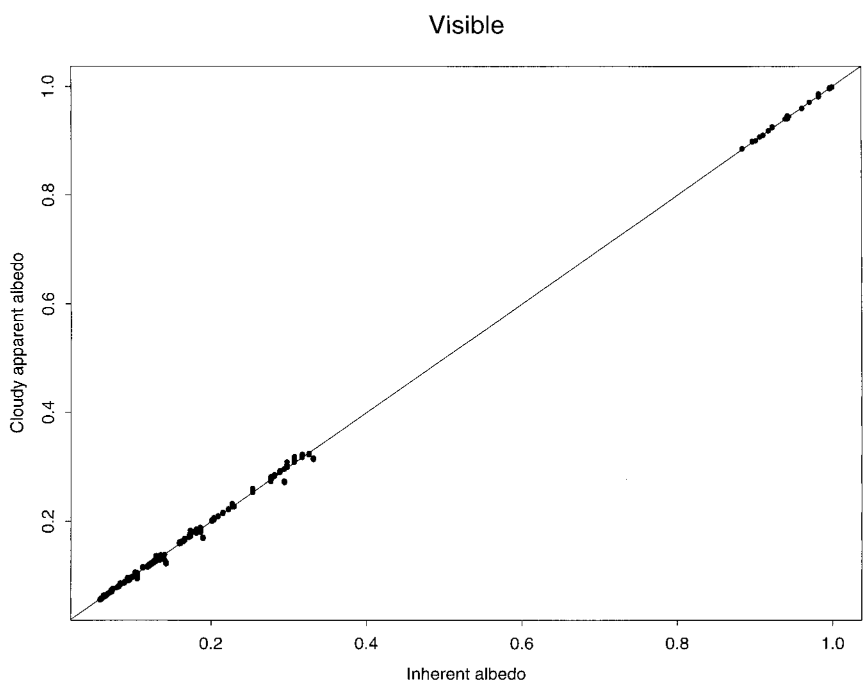

FIG. 5. Prediction of surface visible inherent albedos from MODIS narrowband TOA albedos using the polynomial regression and a neural network.

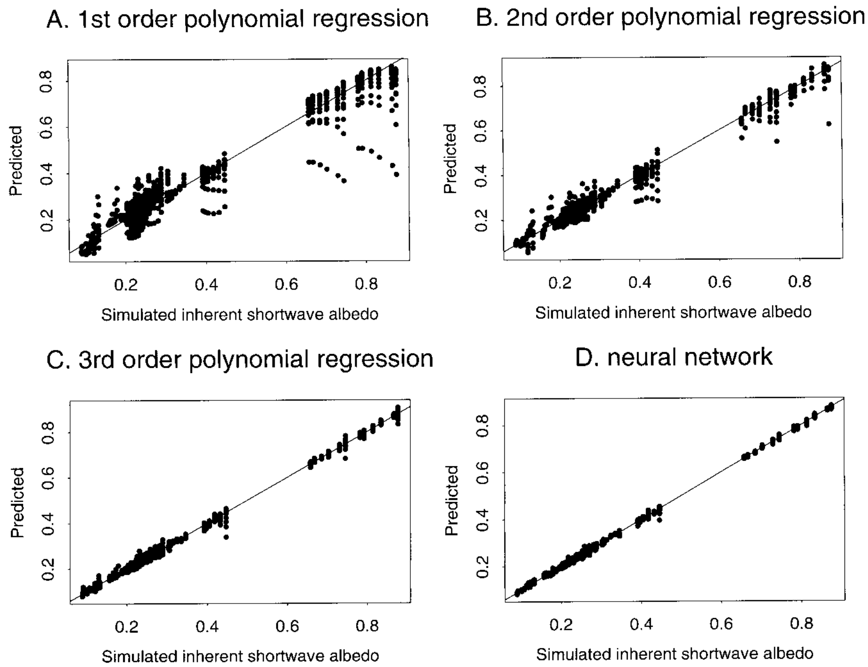

FIG. 6. Surface shortwave apparent albedos and inherent albedos for cloudy conditions.

Lambertian surface. The surface BRF is characterized by an empirical formula (Rahman et al. 1993)

$$R(\theta_i, \phi_i, \theta, \phi) = R_0[\cos\theta_i \cos\theta(\cos\theta_i + \cos\theta)]^{k-1}F(g)B(G),$$

where R_0 and k are two coefficients. Here, $F(g)$ is the Henyey–Greenstein phase function

$$F(g) = \frac{1 - g^2}{[1 + g^2 - 2g\cos(\pi - \Theta)]^{1.5}},$$

where g is the asymmetry parameter and Θ is the phase angle

$$\Theta = \cos^{-1}[\cos\theta_i \cos\theta + \sin\theta_i \sin(\theta)\cos(\phi_i - \phi)].$$

Here, $B(G)$ is defined as

$$B(G) = 1 + \frac{1 - R_0}{1 + G},$$

where the geometric factor G is given by

$$G = [\tan^2\theta_i + \tan^2\theta - 2\tan\theta_i \tan\theta\cos(\phi_i - \phi)]^{1/2}.$$

Here, R_0 is a parameter controlling the overall magnitude of the surface reflectance and $B(G)$ characterizes the hotspot function. The hotspot is a phenomena of reflectance enhancement when the viewing directional coincides with the solar illumination direction. The five sets of parameters of the surface BRF are listed in Table 1.

The non-Lambertian surface is assumed to be underneath an aerosol atmosphere. We use four different aerosol optical depths (0.1, 0.5, 0.8, and 1.2) and four different solar zenith angles (5°, 30°, 60°, and 80°). The aerosol phase function and single-scattering albedo are calculated by Mie theory based on the power laws distribution of aerosol particles. The particle sizes and refractive index match aerosols from biomass burning (Penner et al. 1992). The minimum and maximum radii are 0.007 06 μm and 1.9964 μm, and the refractive index is $(1.43 + i0.0035)$. The reference wavelength is 0.8 μm. The comparison is given in Fig. 2. The surface spectral inherent albedo is based on (1) and apparent albedo on (3). In many cases, different atmospheric conditions in conjunction of different surface BRF produce

TABLE 2. Weights of converting surface MODIS narrowband albedos to broadband albedos.

MODIS bands	Wavelength (nm)	Visible	Near-IR (I)	Near-IR (II)	Shortwave
1	620–670	0.3265	—	—	0.3973
2	841–876	—	0.5447	0.5271	0.2382
3	459–479	0.4364	—	—	0.3489
4	545–565	0.2366	—	—	−0.2655
5	1230–1250	—	0.1363	0.1795	0.1604
6	1628–1652	—	0.0469	—	−0.0138
7	2105–2155	—	0.2536	0.2755	0.0682
intercept	—	−0.0019	−0.0068	−0.0071	0.0036

TABLE 3. Summary of MODIS fitting residuals.

Broadbands	Min	1st-Qu.	Median	3rd-Qu.	Max	RSE
Short	−0.0249	−0.0034	−0.0008	0.0032	0.0393	0.0065
Visible	−0.0044	−0.0010	0.0002	0.0007	0.0052	0.0017
Near-IR(I)	−0.0293	−0.0034	0.0000	0.0029	0.0282	0.0108
Near-IR(II)	−0.0292	−0.00364	−0.0001	0.0026	0.0313	0.0107

apparent albedo outside the envelope of ±0.05 from the inherent albedo because different atmospheric conditions generate different sky radiance distributions. Since we used the same formula (Dickinson 1983) to scale all surface reflectance for different solar zenith angles, one set of the scaled fresh snow reflectance greater than one in this figure may be physically meaningless in reality.

Surface spectral albedos are weighted by the downward irradiance to calculate the apparent broadband albedo. The inherent broadband albedo is weighted by the TOA extraterrestrial downward irradiance so that it is independent of the atmospheric conditions. The spectral distributions of downward irradiance are actually weighting functions to convert the surface spectra into broadband apparent albedos under different atmospheric conditions.

Figure 3a plots inherent albedo and apparent shortwave albedo under the clear-sky conditions for the range of surface spectra, solar zenith angles, visibilities, aerosol models, and water vapor profiles that is described in section 3. We can see that the difference is too large to be ignored. Smaller shortwave albedos have smaller differences between the apparent and inherent albedos. For snow-covered surfaces, the apparent albedos are always larger than the inherent albedos.

It is interesting to note in Fig. 3b that the apparent and inherent albedos under clear-sky conditions in the visible region are almost identical. The reason is probably that when we change the atmospheric parameters, the shapes of the spectral distributions of downward irradiance are very similar although their magnitudes vary greatly in the visible spectral region.

b. Cloudy-sky surface albedos and surface inherent albedos

Under cloudy conditions, the broadband surface albedo is different from that of the clear-sky conditions because the spectral distributions of the downward irradiance at the surface are different. Figure 4 shows the relation between the surface inherent shortwave albedo and shortwave apparent albedo for cloudy sky conditions. Five types of clouds are considered: cumulus, altostratus, stratus, stratus/stratocumulus, and nimbostratus. For snow-covered surfaces, cloudy apparent albedo is always larger than the inherent shortwave albedo. Most other cover types have an opposite trend. It is clear that in most cases cloudy total shortwave apparent albedo is different from clear-sky shortwave apparent albedo as well as shortwave inherent albedo. For visible (Fig. 5) albedo, no significant differences exist.

Note that cumulus clouds are often heterogeneous and MODTRAN, which assumes plane-parallel, only vertical variations, may be unable to simulate the ''true'' situations under such conditions.

TABLE 4. Weights of converting surface MISR narrowband albedos to broadband albedos.

MISR bands	Wavelength (nm)	Visible	Near-IR	Shortwave
1	423–458	0.3511	—	0.1587
2	543–558	0.3923	—	−0.2463
3	663–678	0.2603	—	0.5442
4	853–878	—	0.6088	0.3748
intercept	—	−0.0030	0.1442	0.0149

c. Converting MODIS/MISR narrowband albedos to broadband albedos

There are two ways to estimate surface broadband inherent albedos. One is based on surface narrowband albedos (6). The MODIS science team will generate seven surface narrowband albedos (Strahler et al. 1996). Based on more than 100 surface spectra of vegetation, soil, and snow from the USGS spectra library and the measured spectra provided by Dr. J. Salisbury (20 of which were used for the MODTRAN simulations), it is found that a linear combination of these seven MODIS surface narrowband albedos can predict the total shortwave inherent albedo very accurately. In this process, solar TOA extraterrestrial irradiance from MODTRAN and the MODIS seven-band spectral response functions were used. The coefficients for converting MODIS narrowband surface inherent albedos to the three surface broadband inherent albedos are given in Table 2. MODIS narrowband surface inherent albedos and the three broadband surface inherent albedos were calculated from these surface reflectance spectra and sensor spectral response functions. For estimating near-IR broadband albedo, two sets of coefficients are given. In the first case, all four near-IR narrow bands are used. Since the estimation variance associated with the band-6 coefficient is too large, band 6 is simply dropped in the second case.

The fitting residuals for the MODIS are summarized in Table 3. The terms 1st-Qu. and 3rd-Qu. stand for the first quantile and the third quantile of the residuals. The residual standard errors (RSE) are also given in the last column. RSE indicates the overall fitting for all spectra

TABLE 5. Summary of MISR fitting residuals.

Broadbands	Min	1st-Qu.	Median	3rd-Qu.	Max	RSE
Short	−0.04987	−0.0165	0.0047	0.0112	0.1136	0.0232
Visible	−0.0062	−0.0008	−0.0001	0.0008	0.0068	0.0024
Near-IR	−0.1476	−0.0479	0.0104	0.0389	0.1794	0.0633

and the minimum and maximum show the worse scenarios.

For MISR, the corresponding coefficients are given in Table 4. Although MISR does not have the same number of narrow bands as MODIS, we found that broadband shortwave and visible inherent albedos can be accurately predicted ($R^2 \approx 1.0$), but R^2 for predicting near-IR inherent albedo is only 0.79 simply because only one near-IR waveband is available for estimation. The fitting residuals for the MISR are summarized in Table 5. The largest residual for the near-IR fitting is as large as 0.18. For the total shortwave, the overall RSE is very good, but the worse residual is 0.11. It is not surprising to see that the best results are achieved for the visible band.

The other way of estimating broadband inherent albedos is to use TOA narrowband albedos directly without employing any atmospheric correction. This is the new method that we introduce in this paper. Figure 6 shows two techniques for predicting shortwave albedos from seven MODIS TOA albedos. The first approach is the polynomial regression technique with orders from 1 to 3, and the second is the neural-network technique. It is evident that the first- and second-order polynomial regressions do not predict shortwave inherent albedo well. The third-order polynomial regression performs very well, although the number of coefficients is extremely large. The neural network performs better than the third-order polynomial regression. This demonstrates that a neural network can represent a high-degree nonlinear relation very well.

A similar approach is used for estimating visible inherent albedo using three MODIS narrowband TOA albedos (Fig. 7). However, the prediction is not good enough with either approach. Obviously three bands are not enough to allow us to distinguish between the atmospheric and surface information. However, a primary analysis shows that if aerosol optical depth is known, either approach can predict surface inherent visible albedo very well.

The MISR team will produce TOA albedo products (Diner et al. 1996), but the MODIS team will not. It has been demonstrated (Liang and Townshend 1997) that different techniques are available for this purpose. The impacts of the uncertainties of the TOA albedo products on surface albedo estimations need to be evaluated and quantified in the future.

d. Direct and diffuse albedos

In some energy balance related models (e.g., Koster and Suarez 1992, 1994), albedo is further divided into

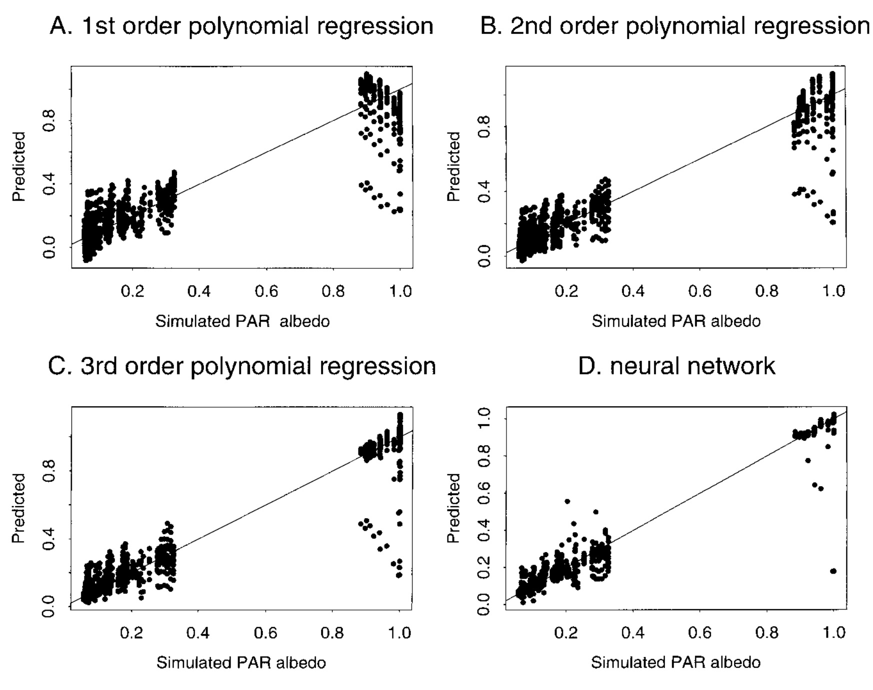

FIG. 7. Surface visible apparent albedo and inherent albedo for cloudy conditions.

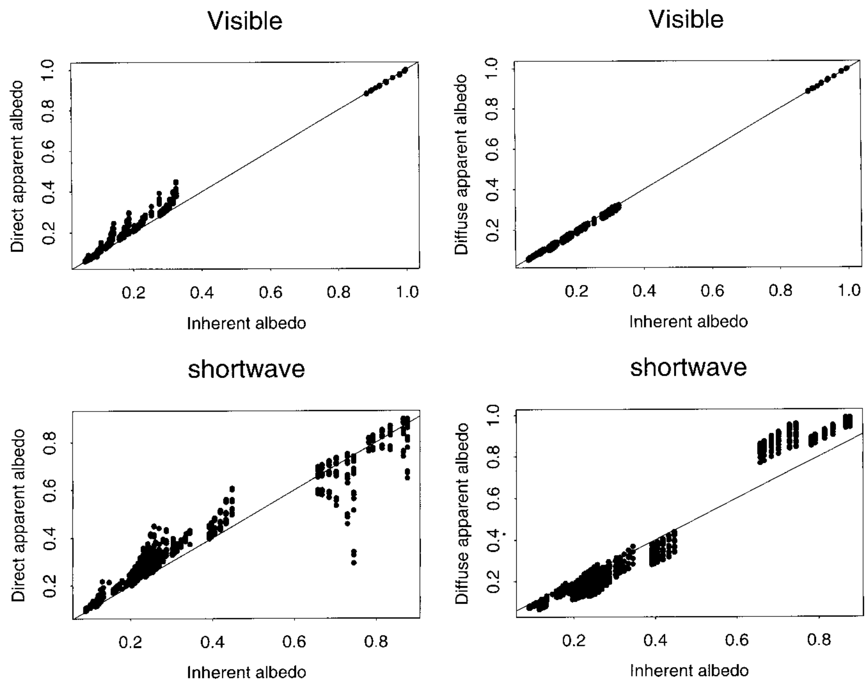

FIG. 8. Direct and diffuse apparent albedos and inherent albedos in both shortwave and visible broad bands.

direct albedo and diffuse albedo. In our simulations (Fig. 8), MODTRAN was modified to output direct and diffuse irradiance separately. From this figure, we can see that direct albedo tends to be larger than diffuse albedo in most cases. The diffuse visible apparent albedo is almost identical to the diffuse inherent visible albedo. For vegetation and soil cover types, direct apparent albedos are larger than inherent albedo and diffuse apparent albedo smaller than inherent albedos in the total shortwave region.

6. Summary and discussions

For climatic modeling and energy balance studies, surface broadband albedos are required. However, surface broadband albedos are not sole measures of the surface reflective properties, as they also depend on the atmospheric conditions. This implies that surface broadband surface albedos retrieved from satellite observations under a specific set of atmospheric conditions may not be suitable for application to other atmospheric conditions.

In this study, we distinguish surface inherent albedo, which is independent of the atmospheric conditions, from apparent albedo. Surface spectral inherent albedo is integrated from surface BRDF; surface spectral apparent albedo is defined as the ratio of the upwelling irradiance to downward irradiance, which depends on the angular distribution of sky radiance. Surface inherent albedo for a given wavelength range is the surface spectral inherent albedo weighted by the extraterrestrial downward spectral irradiance at the top of the atmosphere. Similarly, surface apparent albedo for a certain wavelength range is the surface spectral apparent albedo weighted by downward spectral irradiance at the surface.

Based on extensive radiative transfer simulations with different surface directional reflectances and atmospheric conditions, we found that surface spectral inherent albedos are significantly different from surface spectral apparent albedo in many cases.

We define three broadband surface inherent albedos, total shortwave, visible, and near-infrared, that are completely independent of the atmospheric conditions. Extensive atmospheric radiative transfer simulations with different surface reflectance spectra and atmospheric conditions using MODTRAN show that total shortwave broadband apparent albedos are significantly different from surface inherent shortwave albedos and largely depend on atmospheric conditions. In contrast, the apparent and inherent visible and near-IR albedos are very similar. Regarding direct and diffuse components of albedo, differences between the inherent albedos and apparent direct and diffuse albedos are significant in most cases.

For practical applications, apparent albedos are needed. However, the apparent albedo under one atmospheric condition may not be suitable for applications to other atmospheric conditions. We suggest that surface inherent albedo products be developed from satellite observations. If the linkages between inherent albedo and apparent albedo are established, users can convert inherent albedo to apparent albedo for any specific atmospheric conditions.

We also investigated two approaches for converting narrowband albedos to the broadband albedos. The first approach involves the atmospheric correction procedure that retrieves the surface narrowband albedos from TOA satellite observations. Tables of coefficients are given to convert MODIS and MISR surface narrowband albedos to broadband surface inherent albedos. The dependences are linear. The second approach determines the broadband albedos directly from TOA narrowband albedos without performing any atmospheric correction. For this case, the predictions of shortwave broadband inherent albedo from either MODIS or MISR TOA albedos are very good using either a polynomial regression technique or a feed-forward neural network. However, for visible broadband albedo, the three narrowband TOA albedos from either MODIS or MISR do not contain sufficient information to allow us to derive inherent albedo accurately. There is a need to incorporate atmospheric parameters into the prediction procedure.

This study is partially based on several assumptions made in the MODTRAN radiative transfer simulations. The first one is that the surface is Lambertian, that is, surface reflectance is isotropic when we calculate broadband albedos. This limitation arises because MODTRAN was run for every wavenumber in the whole shortwave region (0.25–5 μm). BRDF models or observations with this wavelength range are simply unavailable for our broad selection of cover types. To make simulations more realistic, surface reflectance spectra were scaled so that different surface reflectance spectra were input to MODIS at different solar zenith angles. Incorporating any real surface BRDF probably will not change the conclusions drawn in this study. The second assumption is that the adjacency effect is negligible. For MODIS and MISR 1-km products, this is a valid assumption. For some 250-m products over highly complicated landscapes, the adjacency effect may have to be considered (Hu et al. 1998). Future research will focus on these issues.

Acknowledgments. We thank Drs. Lex Berk and Gail Anderson for their kind help in modifying MODTRAN codes and Dr. Frank Evans for providing the SHDOM code and other generous assistance. The authors are also grateful to Dr. J. Salisbury for providing surface spectra measurement data, and Drs. Wolfgang Lucht, Zhanqing Li, and Crystal Schaaf for valuable discussions. We also thank anonymous referees for their careful and constructive reviews. This study was supported in part by the National Aeronautics and Space Administration under Grant NAG56459 and Contract NAS-5-31369.

REFERENCES

Abuelgasim, A. A., S. Gopal, and A. H. Strahler, 1996: Classification of ASAS multiangle and multispectral measurements using artificial neural networks. *Remote Sens. Environ.,* **57,** 79–87.

Anderson, G. P., 1996: MODTRAN 3 user instructions. U.S. Air Force Geophysics Laboratory, 37 pp. [Available from Geophysics Laboratory, U.S. Air Force, Hanscom AFB, MA 01731-5000.]

Atkinson, P. M., and A. R. L. Tatnall, 1997: Introduction: Neural networks in remote sensing. *Int. J. Remote Sens.,* **18,** 699–709.

Bastable, H., W. Shuttleworth, R. Dallarosa, G. Fisch, and C. Nobre, 1993: Observations of climate, albedo, and surface radiation over cleared and undisturbed Amazonian forest. *Int. J. Climatol.,* **13,** 783–796.

Berk, A., L. Bernstein, and D. Robertson, 1989: MODTRAN: A moderate resolution model for LOWTRAN 7. U.S. Air Force Geophysics Laboratory Tech. Rep. GL-TR-89-0122, 37 pp. [Available from Geophysics Laboratory, U.S. Air Force, Hanscom AFB, MA 01731-5000.]

Cess, R. D., 1978: Biosphere-albedo feedback and climate modeling. *J. Atmos. Sci.,* **35,** 1765–1768.

Chen, T. S., and G. Ohring, 1984: On the relationship between clear-sky planetary and surface albedos. *J. Atmos. Sci.,* **41,** 156–158.

Clark, R. N., G. A. Swayze, A. J. Gallagher, T. V. V. King, and W. M. Calvin, 1993: The U.S. Geological Survey digital spectral library: Version 1: 0.2 to 3.0 microns. U.S. Geological Survey Open File Rep. 93-592, 1340 pp. [Available online at http://speclab.cr.usgs.gov/spectral-lib.html.]

Dickinson, R. E., 1983: Land surface processes and climate-surface albedos and energy balance. *Advances in Geophysics,* Vol. 25, Academic Press, 305–353.

Diner, D. J., 1996: MISR Level 2 Surface Retrieval Algorithm theoretical basis. JPL D-11401, Rev. B., 78 pp.

——, R. Davies, T. Varnai, C. Borel, and S. Gerstl, 1996: MISR Level 2 Top-of-Atmosphere Albedo Algorithm theoretical basis. JPL D-13401, Rev. B, 88 pp.

Dorman, J. L., and P. J. Sellers, 1989: A global climatology of albedo, roughness length and stomatal resistance for atmospheric general circulation models as represented by the Simple Biosphere model SiB. *J. Appl. Meteor.,* **28,** 833–855.

Evans, K. F., 1998: The spherical harmonics discrete ordinate method for three-dimensional atmospheric radiative transfer. *J. Atmos. Sci.,* **55,** 429–464.

Foody, G. M., R. M. Lucas, P. J. Curran, and M. Honzak, 1997: Nonlinear mixture modeling without end-members using an artificial neural network. *Int. J. Remote Sens.,* **18,** 937–953.

Hu, B., W. Lucht, and A. Strahler, 1998: The interrelationship of atmospheric correction of reflectance and surface BRDF retrieval: A sensitivity study. *IEEE Trans. Geosci. Remote Sens.,* in press.

Kimes, D. S., and B. N. Holben, 1992: Extracting spectral albedo from *NOAA-0* AVHRR multiple view data using an atmospheric correction procedure and an expert system. *Int. J. Remote Sens.,* **13,** 275–289.

Koepke, P., and K. T. Kriebel, 1987: Improvements in the shortwave cloud-free radiation budget accuracy. Part I: Numerical study including surface anisotropy. *J. Climate Appl. Meteor.,* **26,** 374–395.

Koster, R., and M. Suarez, 1992: Modeling the land surface boundary in climate models as a composite of independent vegetation stands. *J. Geophys. Res.,* **97,** 2697–2715.

——, and ——, 1994: The components of a SVAT scheme and their effects on a GCM's hydrological cycle. *Adv. Water Resour.,* **17,** 61–78.

Li, Z., and L. Garand, 1994: Estimation of surface albedo from space: A parameterization for global application. *J. Geophys. Res.,* **99,** 8335–8350.

Liang, S., and A. H. Strahler, 1994: Retrieval of surface BRDF from multiangle remotely sensed data. *Remote Sens. Environ.,* **50,** 18–30.

——, and P. Lewis, 1996: A parametric radiative transfer model for sky radiance distribution. *J. Quant. Spectrosc. Radiat. Transfer,* **55,** 181–189.

——, and J. R. G. Townshend, 1996a: A modified Hapke model for soil bidirectional reflectance. *Remote Sens. Environ.,* **55,** 1–10.

——, and ——, 1996b: A parametric soil BRDF model: A four stream approximation for multiple scattering. *Int. J. Remote Sens.,* **17,** 1303–1315.

——, and ——, 1997: Angular signatures of NASA/NOAA Pathfinder AVHRR land data and applications to land cover identification. *Proc. IGARSS'97,* Vol. 4, Singapore, IGARSS, 1781–1783.

Lindner, B. L., 1988: Ozone on Mars: The effects of clouds and airborne dust. *Planet. Space Sci.,* **36,** 125–144.

Loehrer, S. M., T. A. Edmands, and J. A. Moore, 1996: TOGA COARE upper-air sounding data archive: Development of quality control procedures. *Bull. Amer. Meteor. Soc.,* **77,** 2651–2671.

Lummerzheim, D., W. R. Rees, and H. R. Anderson, 1989: Angular dependent transport of auroral electrons in the upper atmosphere. *Planet. Space Sci.,* **37,** 109–129.

Penner, J. E., R. E. Dickinson, and C. A. O'Neill, 1992: Effects of aerosol from biomass burning on the global radiation budget. *Science,* **256,** 1432–1434.

Pinker, R. T., 1985: Determination of surface albedo from satellite. *Adv. Space Res.,* **5,** 333–343.

Palluconi, F., G. Hoover, R. Alley, M. Jentoft-Nilsen, and T. Thompson, 1996: An atmospheric correction method for ASTER thermal radiometry over land. Rev. 2, NASA/EOS ATBD, 26 pp.

Pinty, B., and D. Ramond, 1987: A method for the estimate of broadband surface albedo from a geostationary satellite. *J. Climate Appl. Meteor.,* **26,** 1709–1722.

Rahman, H., M. M. Verstraete, and B. Pinty, 1993: Coupled surface-atmosphere reflectance (CSAR) model, 1. Model description and inversion on synthetic data. *J. Geophys. Res.,* **98,** 20 779–20 790.

Ranson, K. J., J. R. Irons, and C. S. T. Daughtry, 1991: Surface albedo from bidirectional reflectance. *Remote Sens. Environ.,* **35,** 201–211.

Sato, N., P. J. Sellers, D. A. Randall, E. K. Schneider, J. Shukla, J. L. Kinter III, Y. T. Hou, and E. Albertazzi, 1989: Effects of implementing the Simple Biosphere model (SiB) in the general circulation model. *J. Atmos. Sci.,* **46,** 2757–2782.

Stamnes, K., S. C. Tsay, W. Wiscombe, and K. Jayaweera, 1988: Numerically stable algorithm for discrete-ordinate-method radiative transfer in multiple scattering and emitting layered media. *Appl. Opt.,* **27,** 2502–2509.

Strahler, A. H., W. Wanner, C. Schaaf, X. Li, B. Hu, J.-P. Muller, P. Lewis, and M. Barnsley, 1996: MODIS BRDF/albedo product: Algorithm theoretical basis documentation. Version 4.0, NASA/EOS ATBD, 94 pp.

Tsay, S. C., and K. Stamnes, 1992: Ultraviolet radiation in the Arctic: The impact of potential ozone depletions and cloud effects. *J. Geophys. Res.,* **97,** 7829–7840.

——, ——, and K. Jayaweera, 1989: Radiative energy budget in the cloudy and hazy arctic. *J. Atmos. Sci.,* **46,** 1002–1018.

Venables, W. N., and B. D. Ripley, 1994: *Modern Applied Statistics with S-Plus.* Springer-Verlag, 461 pp.

Walthall, C. L., J. M. Norman, J. M. Welles, G. Campbell, and B. L. Blad, 1985: Simple equation to approximate the bidirectional reflectance from vegetation canopies and bare soil surfaces. *Appl. Opt.,* **24,** 383–387.

Wan, Z, 1996: MODIS Land Surface Temperature Algorithm theoretical basis documentation. NASA/EOS ATBD, 71 pp.

Wielicki, B. A, and B. R. Barkstrom, 1996: Clouds and the Earth's Radiant Energy System (CERES) Algorithm theoretical basis document. NASA/EOS ATBD, 21 pp.